Analytical and Bioanalytical Chemistry (2020) 412:2743–2754
https://doi.org/10.1007/s00216-020-02538-3

PAPER IN FOREFRONT

Fluorescence quenching of the SYBR Green I-dsDNA complex by in situ generated magnetic ionic liquids

Ashley N. Bowers[1] · Kalyan Santra[1] · María J. Trujillo-Rodríguez[1] · Anthony Song[1] · Miranda N. Emaus[1] · Jacob W. Petrich[1] · Jared L. Anderson[1]

Received: 17 January 2020 / Revised: 17 February 2020 / Accepted: 20 February 2020 / Published online: 22 April 2020

Abstract

Magnetic ionic liquids (MILs) with metal-containing cations are promising extraction solvents that provide fast and high efficiency extraction of DNA. Hydrophobic MILs can be generated in situ in a methodology called in situ dispersive liquid-liquid microextraction. To consolidate the sample preparation workflow, it is desirable to directly use the DNA-enriched MIL microdroplet in the subsequent analytical detection technique. Fluorescence-based techniques employed for DNA detection often utilize SYBR Green I, a DNA binding dye that exhibits optimal fluorescence when bound to double-stranded DNA. However, the MIL may hinder the fluorescence signal of the SYBR Green I-dsDNA complex due to quenching. In this study, MILs with metal-containing cations were selected and their fluorescence quenching effects evaluated using Förster Resonance Energy Transfer and quantified using Stern-Volmer models. The MILs were based on N-substituted imidazole ligands (with butyl- and benzyl- groups as substituents) coordinated to Ni^{2+} or Co^{2+} metal centers as cations, and paired with chloride anions. The effects of $NiCl_2$ and $CoCl_2$ salts and of the 1-butyl-3-methylimidazolium chloride ionic liquid on the fluorophore complex were also studied to understand the components of the MIL structure that are responsible for quenching. The metal within the MIL chemical structure was found to be the main component contributing to fluorescence quenching. Förster critical distances between 11.9 and 18.8 Å were obtained for the MILs, indicating that quenching is likely not due to non-radiative energy transfer but rather to spin-orbit coupling or excited-state electron transfer. The MILs were able to be directly used in qPCR and fluorescence emission measurements using a microplate reader for detection, demonstrating their applicability in fluorescence-based detection methods.

Keywords DNA · In situ magnetic ionic liquids · Fluorescence spectroscopy · Fluorescence quenching · Fluorescence resonance energy transfer · Stern-Volmer relationship

Introduction

DNA analysis is central to many applications in clinical diagnostics [1], personalized medicine [2], forensics [3], and archaeology [4]. The majority of DNA analysis methodologies use polymerase chain reaction (PCR) [5] and fluorescence-based assays [6]. In quantitative PCR (qPCR), the amplified DNA binds to a fluorescent dye, such as SYBR Green I, and the amount of amplified DNA can be monitored in real-time by the increase in the fluorescent signal of the dye-DNA fluorophore complex [7].

In performing both PCR and fluorescence-based DNA analysis, sample pretreatment steps are generally required to extract and purify DNA from the biological matrix. Small amounts of contaminating species (such as other nucleic acids, proteins) and the quality of the DNA obtained can affect the reliability of the results and DNA obtained for use in downstream applications [8, 9]. Traditional DNA extraction protocols such as the phenol-chloroform liquid-liquid extraction method use large amounts of toxic solvents, lack selectivity, and involve numerous steps resulting in variable amounts of recovered DNA [8, 10]. Many commercially available kits that have been developed to circumvent these issues contain

Electronic supplementary material The online version of this article (https://doi.org/10.1007/s00216-020-02538-3) contains supplementary material, which is available to authorized users.

✉ Jared L. Anderson
andersoj@iastate.edu

[1] Department of Chemistry, Iowa State University, 1605 Gilman Hall, Ames, IA 50011, USA

a solid-phase support such as silica, cellulose magnetic particles, or an anion-exchange resin [8]. These kits, however, often have limited reusability, are expensive, and may require specific equipment.

As an alternative to the aforementioned traditional DNA extraction methods, ionic liquids (ILs) and, more recently, magnetic ionic liquids (MILs) have been increasingly studied for the extraction and preservation of nucleic acids [11–17]. ILs are molten salts composed solely of ions with melting points below 100 °C [18]. ILs have tunable physical and chemical properties [18]. MILs are a subclass of ILs that contain a paramagnetic component in their cationic and/or anionic moiety allowing MIL droplets to be collected with a strong external magnet, replacing time-consuming centrifugation steps [19–22]. MILs possess many of the same advantageous properties of ILs such as low vapor pressure at room temperature, variable viscosity, unique solvation capabilities for both hydrophilic and hydrophobic compounds, and high electrical conductivity [23]. The cation and anion of the IL and/or MIL structure can be tuned for specific applications and interactions with certain analytes. This has led to the design of IL and MIL-based extraction methods that provide high extraction efficiencies for DNA [12, 13, 24].

The majority of the MILs employed in DNA extractions have contained the paramagnetic component in the anion [13, 15]. However, in a recent report MILs possessing paramagnetic cations were investigated for the extraction of DNA [24]. This class of MILs, initially soluble in aqueous solution, was able to undergo a metathesis reaction during the extraction to generate a hydrophobic MIL in situ, thereby facilitating the rapid extraction of DNA. These MILs extracted 20 bp DNA, ~ 250–500 bp DNA, and ~ 20 kbp DNA with high extraction efficiencies (> 42%) using in situ dispersive liquid-liquid microextraction in combination with indirect detection methods [24].

When MIL-based DNA extractions are directly combined with PCR, customized buffers are usually designed to alleviate PCR inhibition caused by cationic and anionic components of the MIL [15, 25]. Despite the use of these buffers, quantitative PCR was not possible in the case of MILs containing Fe(III)-anions due to quenching of the fluorescence signal [26]. To understand more thoroughly the role of chemical components that make up MILs in fluorescence-based applications, fluorescence quenching mechanisms can be examined using Förster Resonance Energy Transfer (FRET) or quantified using Stern-Volmer models [26]. FRET evaluates the non-radiative energy transfer from a fluorescent donor to a ground-state acceptor as defined by the overlap integral [26, 27]. Stern-Volmer plots represent the fluorescence signal when increasing concentration of quencher is added and constitute a method commonly used to determine the magnitude and nature of fluorescence quenching [26, 28, 29]. In a previously published study, both FRET and Stern-Volmer models were applied to MILs containing phosphonium cations and paramagnetic anion complexes in which different metals were coordinated with hexafluoroacetylacetonate (hfacac) ligands. Cyanine5 carboxylic acid (Cy5) was employed as the fluorophore in this study, which is fluorescent in both its native form and when tagged to DNA. The authors found that Fe(III)- and Co(II)-based MILs strongly quenched the fluorescence signal [26]. Quenching, however, was much less pronounced with MILs containing Mn(II), and they were deemed to be more compatible for direct use in fluorescence-based assays [26]. Other paramagnetic metal complexes have also been shown to quench fluorescence signals in different studies [30, 31]. With regard to MILs containing paramagnetic cations, no studies have yet explored fluorescence quenching in these systems.

In this study, fluorescence quenching of the SYBR Green I-double-stranded DNA (dsDNA) complex by a new generation of MILs containing paramagnetic cations was investigated. The MILs studied contained four N-substituted imidazole ligands (N-butylimidazole or N-benzylimidazole) coordinated to Ni^{2+} or Co^{2+} metal centers and chloride anions. The use of the selected fluorophore complex (SYBR Green I-dsDNA) provided an environment similar to fluorescence-based DNA detection methods. FRET and fluorescence quenching studies using Stern-Volmer models were performed to evaluate the quenching effects of the MILs in the system. $NiCl_2$ and $CoCl_2$ salts as well as the 1-butyl-3-methylimidazolium chloride ($[BMIm^+][Cl^-]$) IL were employed as controls to better understand the components of the MIL structure that are responsible for quenching.

Experimental

Chemicals, reagents, and materials

Double-stranded DNA (dsDNA; ~ 20 kbp salmon testes DNA) used in this study was purchased from Sigma-Aldrich (St. Louis, MO, USA). SYBR Green I (10,000×) was purchased from Life Technologies (Eugene, OR, USA). Tris(hydroxymethyl)aminomethane (Tris base) was purchased from Research Products International (Mount Prospect, IL, USA). Ultrapure water (18.2 MΩ·cm) was obtained from a Milli-Q water purification system (Millipore, Bedford, MA, USA). Disposable cuvettes made of poly(methyl methacrylate) (PMMA) and hydrochloric acid (ACS grade, 36.5–38.0%) were purchased from Fisher Scientific (Fair Lawn, NJ, USA).

For the synthesis of the IL and MILs, the reagents cobalt(II) chloride (97%), 1-butylimidazole (98%), 1-

chlorobutane (99%), and 1-methylimidazole (99%) as well as HPLC-grade ethyl acetate were purchased from Sigma-Aldrich. Nickel(II) chloride (98%) and benzylimidazole (99%) were purchased from Acros Organics (Morris Plains, NJ, USA). Anhydrous diethyl ether (99.0%) was purchased from Avantor Performance Materials Inc. (Center Valley, PA, USA). Deuterated dimethyl sulfoxide-d6 (DMSO-*d6*, 99.9%) was purchased from Cambridge Isotope Laboratories (Andover, MA, USA).

Chemical structures of the IL, MILs, and SYBR Green I dye used are shown in Fig. 1. Stock solutions of the MILs, IL, and metal salts were prepared in 10 mM Tris-HCl buffer (pH 8) at the following concentrations: 10 mM, 1 mM and 0.1 mM for $NiCl_2$, $CoCl_2$, tetra(benzylimidazole)nickel (II) chloride ($[Ni(BnIm)_4^{2+}]2[Cl^-]$) and tetra(butylimidazole)cobalt (II) chloride ($[Co(BIm)_4^{2+}]2[Cl^-]$), 16 mM, 1 mM and 0.1 mM for tetra(butylimidazole)nickel (II) chloride ($[Ni(BIm)_4^{2+}]2[Cl^-]$) and 110 mM, 10 mM and 1 mM for $[BMIm^+][Cl^-]$. Stock solutions of the dsDNA and SYBR Green I were also prepared in Tris-HCl buffer at concentrations of 154 nM and 98 μM, respectively.

Instrumentation and methods

Steady-state absorption and fluorescence spectra were obtained using an Agilent Technologies 8453 UV-visible spectrophotometer and an Agilent Cary Eclipse fluorescence spectrophotometer (Santa Clara, CA, USA), respectively. Emission spectra were obtained with 1-nm resolution and corrected for lamp spectral intensity and detector response. The excitation and emission slit widths were 5 nm and the photomultiplier (PMT) detector voltage was 550 V. The samples were excited at 475 nm with the emission intensity recorded from 485 to 700 nm.

The $[BMIm^+][Cl^-]$ IL was synthesized and purified following a previously reported procedure [32]. The final product was characterized by ^{1}H-NMR, with the spectrum recorded in DMSO-*d6* using a Bruker DRX 500 MHz nuclear magnetic resonance (NMR) spectrometer (Billerica MA, USA) (see Fig. S1 of the Electronic Supplementary Material, ESM). The MILs were synthesized and purified using previously reported methods [33].

One-centimeter path length PMMA cuvettes were used for fluorescence quenching experiments. All samples were prepared in 10 mM Tris-HCl buffer (pH 8) and the total volume,

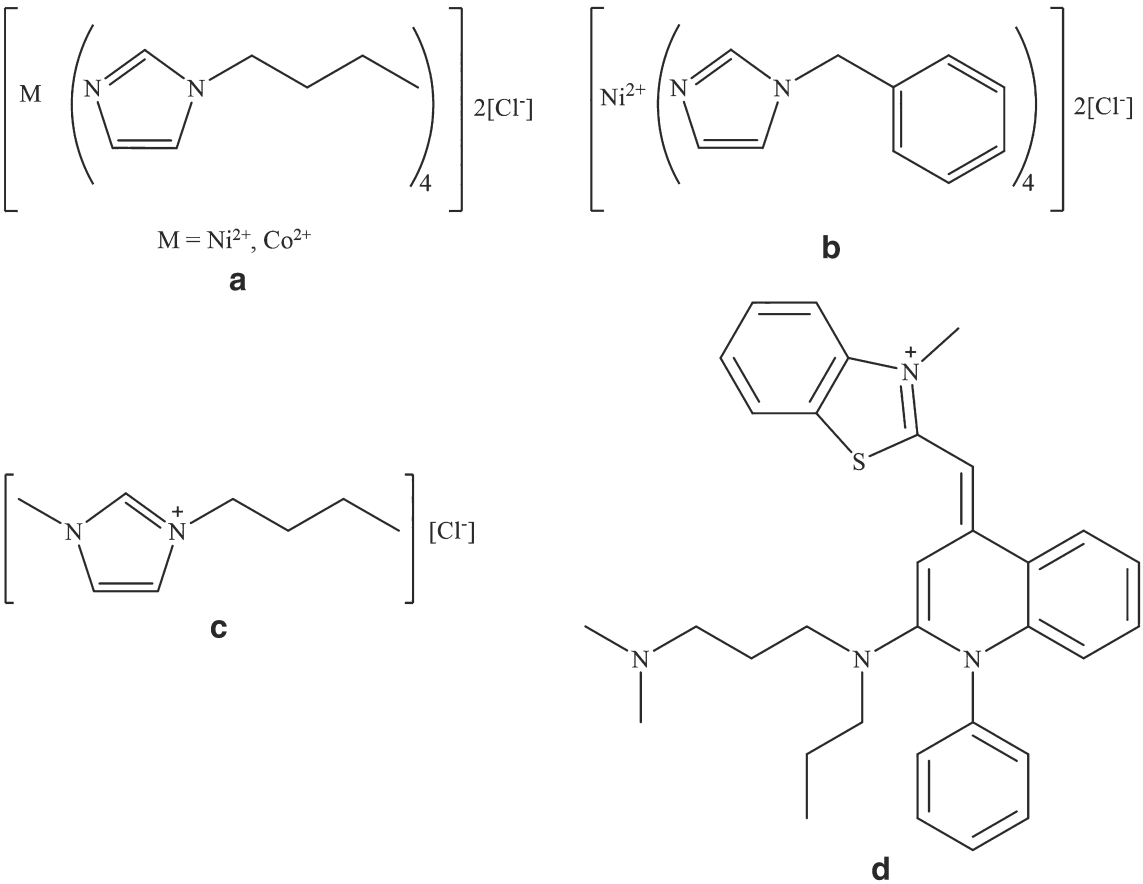

Fig. 1 Chemical structures of the MILs, IL, and fluorophore used in this study. **a** $[Ni(BIm)_4^{2+}]2[Cl^-]$ and $[Co(BIm)_4^{2+}]2[Cl^-]$, **b** $[Ni(BnIm)_4^{2+}]2[Cl^-]$, **c** $[BMIm^+][Cl^-]$, and **d** SYBR Green I

dsDNA concentration, and SYBR Green I concentration were kept constant at 2 mL, 1 nM, and 1.96 μM, respectively. Stock solutions referred to in the "Chemicals, reagents, and materials" section were used to prepare the samples and were prepared in triplicate the same day as the experiment by mixing for 15 s using a vortex (Fisher Scientific). The exception was the dsDNA stock solution, which was stored in 10-mM Tris-HCl buffer at 4 °C. The samples were prepared over a range of increasing concentration of the quenchers. The concentration of the $NiCl_2$ and $CoCl_2$ salts ranged from 0 to 0.5 mM. The concentration of the $[Ni(BIm)_4^{2+}]2[Cl^-]$ and $[Ni(BnIm)_4^{2+}]2[Cl^-]$ MILs varied from 0 to 15 mM and 0 to 2 mM, respectively. The $[Co(BIm)_4^{2+}]2[Cl^-]$ MIL concentration ranged from 0 to 0.5 mM and the concentration of the $[BMIm^+][Cl^-]$ IL from 0 to 100 mM.

To investigate the applicability of the MILs in both qPCR and fluorescence emission spectroscopy using a plate reader for detection, aqueous solutions containing different concentrations of MIL (e.g., 0 to 15 mM of $[Ni(BIm)_4^{2+}]2[Cl^-]$, 0 to 2 mM $[Ni(BnIm)_4^{2+}]2[Cl^-]$, or 0 to 0.5 mM $[Co(BIm)_4^{2+}]2[Cl^-]$) were placed into a Bio-Rad CFX Connect real-time thermocycler (Hercules, CA, USA) and a BioTek Synergy H1 Multi-Mode microplate reader (Winooski, VT, USA), respectively. Each sample also contained 1-nM dsDNA and 1.96 μM of SYBR Green I. In qPCR, the samples were incubated at 25 °C for 30 s before the optical detection step. A 384-well, black, polystyrene, flat bottom microplate (Corning, Corning, NY, USA) was used for fluorescence emission measurements using a microplate reader with an excitation wavelength of 475 nm. The emission intensity was measured from 505 to 650 nm in top-read mode with 1-nm resolution.

Results and discussion

Quantifying fluorescence quenching of the SYBR Green I-DNA complex

Fluorescence quenching can be induced by a variety of molecular interactions such as excited-state reactions, complex formation, energy transfer, and collisional quenching [28]. Collisional (or dynamic) quenching occurs as a result of collisions between an excited-state fluorophore and quencher molecules [34]. On the other hand, a reaction between the quencher in the ground-state and the fluorophore resulting in ground-state complex formation is defined as static quenching [34]. These types of mechanisms are commonly quantified by Stern-Volmer equations [28, 35–37]. Collisional quenching or static quenching is described by Eq. (1):

$$\frac{F_0}{F} = 1 + K_{SV}[Q] \tag{1}$$

where F_0 is the integrated fluorescence intensity of the corrected spectra when the concentration of quencher is 0, F is the integrated fluorescence intensity of the corrected spectra when the concentration of the quencher is $[Q]$, and K_{SV} is the Stern-Volmer quenching constant. If the Stern-Volmer plot of F_0/F versus $[Q]$ is linear, K_{SV} can be directly from the slope of the plot, whose "y-intercept" is 1. In general, when Eq. (1) is applicable, a single class of fluorophores displays a linear Stern-Volmer plot, all of which have equal accessibility to the quencher.

A deviation from linearity towards the "x-axis" for a plot of F_0/F versus $[Q]$ is observed when at two (or more) populations of fluorophores have different accessibility to the quencher, e.g., one more accessible fraction, a, and another less accessible (buried) fraction, b. The total fluorescence in the absence of the quencher, F_0, is equal to that of the two fractions, Eq. (2) [28, 35, 38]:

$$F_0 = F_{0a} + F_{0b} \tag{2}$$

This type of quenching is described by a modified form of the Stern-Volmer equation, Eq. (3) [28, 35, 38]:

$$\frac{F_0}{F_0 - F} = \frac{1}{f_a K_a [Q]} + \frac{1}{f_a} \tag{3}$$

where F_0 and F are the integrated fluorescence intensities of the corrected spectra when the concentration of the quencher is 0 and $[Q]$, respectively. K_a is the Stern-Volmer quenching constant of the accessible fraction, and f_a is the accessible fraction of fluorescence available to the quencher. K_a and f_a can be determined from a plot of $F_0/(F_0-F)$ versus $1/[Q]$, which should be linear, with f_a^{-1} as the "y-intercept" and $(f_a K_a)^{-1}$ as the slope.

For quantifying fluorescence quenching of the SYBR Green I-dsDNA complex, Stern-Volmer plots were constructed using $NiCl_2$ and $CoCl_2$, as well as the $[Ni(BIm)_4^{2+}]2[Cl^-]$, $[Ni(BnIm)_4^{2+}]2[Cl^-]$, and $[Co(BIm)_4^{2+}]2[Cl^-]$ MILs. These are shown in Figs. 2, 3, and 4 and ESM Figs. S2-S3. They are fit to the modified Stern-Volmer equation, Eq. (3), and the results will be discussed in the following sections.

Evaluation of the contribution of Förster resonance energy transfer (FRET) to fluorescence quenching

The rate of non-radiative energy transfer, k_T, from a donor to an acceptor was defined by Förster by means of Eq. (4) [26, 27, 39]:

$$k_T = \frac{1}{\tau_D}\left(\frac{R_0}{R}\right)^6 \tag{4}$$

where R is the distance between the donor and acceptor molecules, τ_D is the fluorescence lifetime of the donor, and R_0 is

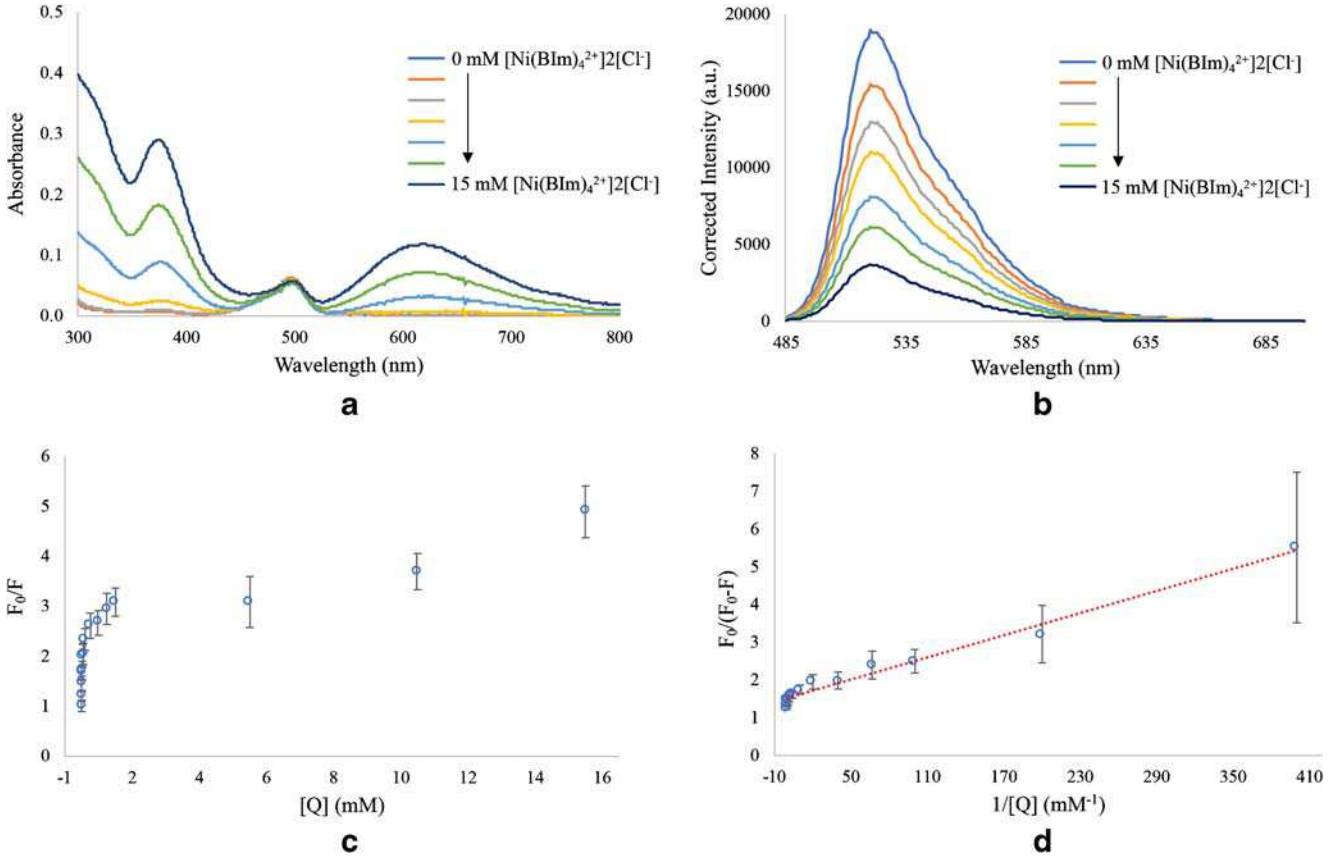

Fig. 2 Fluorescence quenching of the SYBR Green I-dsDNA complex as a function of $[Ni(BIm)_4^{2+}]2[Cl^-]$ concentration. **a** Absorption spectra. **b** Fluorescence emission spectra, $\lambda_{ex} = 475$ nm. Intensities were corrected for the absorption at the wavelength of excitation. **c** Steady-state Stern-Volmer plot of the integrate fluorescence intensity ratio (F_0/F) as a function of quencher concentration. **d** Steady-state modified Stern-Volmer plot of the integrated fluorescence intensity ratio ($F_0/(F_0-F)$) and as a function of $1/[Q]$

the Förster critical transfer distance, defined by Eq. (5):

$$R_0^6 = \frac{9000\ln(10)\phi_D\kappa^2}{128\pi^5 n^4 N_A}\int_0^\infty \frac{F_D\left(\tilde{\nu}\right)\varepsilon_A\left(\tilde{\nu}\right)}{\tilde{\nu}^4}d\tilde{\nu} \quad (5)$$

where ϕ_D is the quantum yield of donor fluorescence emission, κ^2 is the orientation factor and is equal to 2/3 for randomly oriented molecules, n is the solvent refractive index, N_A is Avogadro's number, $F_D(\tilde{\nu})$ is the donor fluorescence emission intensity normalized to unit area on a wavenumber scale, and $\varepsilon_A(\tilde{\nu})$ is the molar decadic extinction coefficient at wavenumber, $\tilde{\nu}$. Non-radiative energy transfer can be determined by the overlap integral of the fluorescence emission spectrum of the donor and the absorbance spectrum of the acceptor, which is evaluated using R_0.

As representative examples, overlap of the fluorescence emission spectrum of the SYBR Green I-dsDNA complex and the absorbance spectrum of $NiCl_2$, $CoCl_2$, $[Ni(BIm)_4^{2+}]2[Cl^-]$, $[Ni(BnIm)_4^{2+}]2[Cl^-]$ and $[Co(BIm)_4^{2+}]2[Cl^-]$ are shown in Fig. S4 of the ESM, whereas the obtained R_0 values are given in Table 1. The R_0 values for the metal salts and the MILs were between 9.00 and 18.8 Å. When compared to the previous generation of MILs containing phosphonium cations and metal chloride or metal hfacac-based anions with Cy5 as the fluorescent donor, R_0 values ranging from 14.2 to 58.1 Å were obtained for the metal salts and the MILs. Out of the studied quenchers, the highest overlap integral was observed for the Co(II) salt (with Cl^- added to achieve a tetrahedral geometry around the metal), indicating a significant contribution of fluorescence quenching through non-radiative energy transfer was possible. In the current study, R_0 values lower than 20 Å were obtained for all of the metal salts and MILs, which suggests that non-radiative energy transfer is not an important process in the fluorescence quenching of the SYBR Green I-dsDNA complex. Therefore, the ability of the metal salts and this new generation of MILs to quench the fluorescence of SYBR Green I-dsDNA is most likely a result of either spin-orbit coupling or excited-state electron transfer or both. It is beyond the focus of the current investigation to attempt to distinguish between the two mechanisms. The most important point is that it was possible to demonstrate that we could evaluate the effect of the metal salts and the MILs on the SYBR Green I-

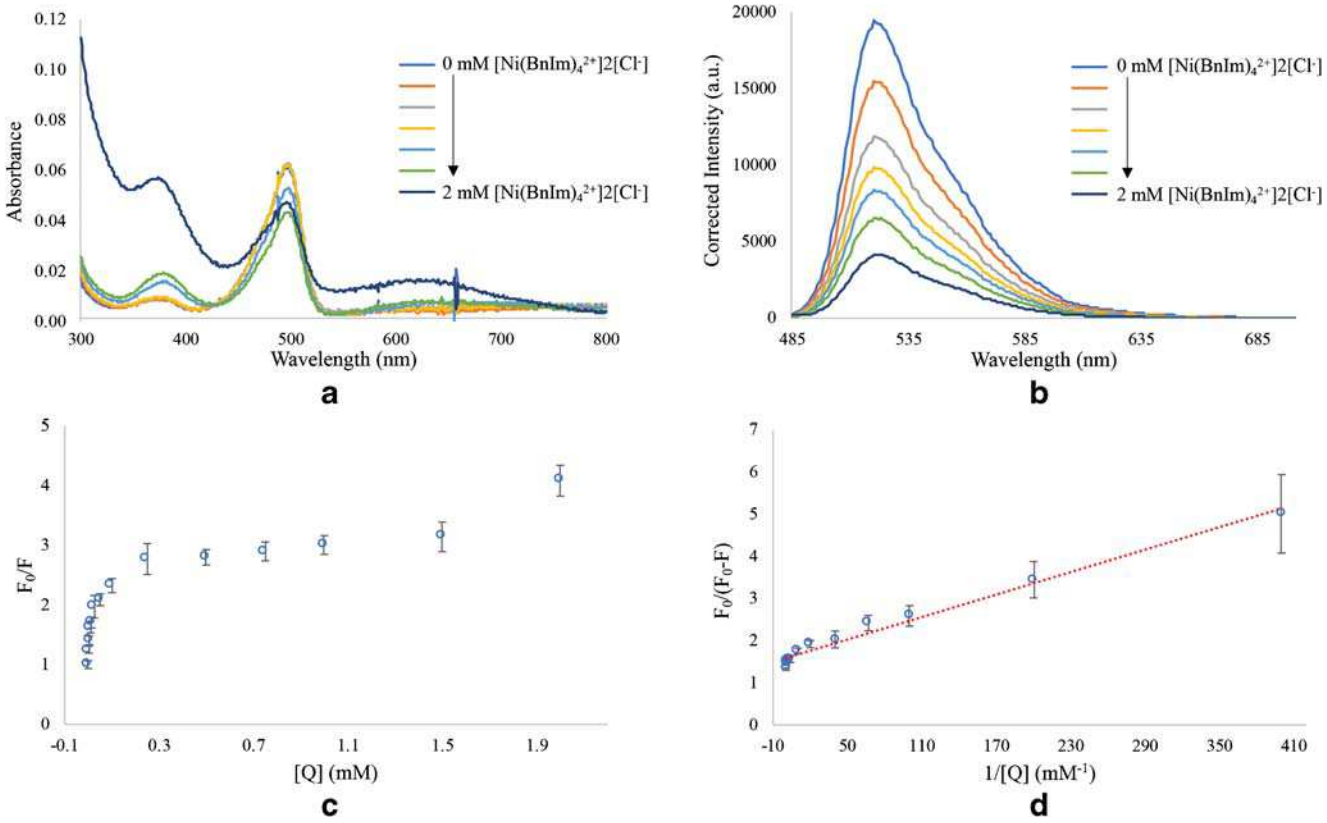

Fig. 3 Fluorescence quenching of the SYBR Green I-dsDNA complex as a function of $[Ni(BnIm)_4^{2+}]2[Cl^-]$ concentration. **a** Absorption spectra. **b** Fluorescence emission spectra, $\lambda_{ex} = 475$ nm. Intensities were corrected for the absorption at the wavelength of excitation. **c** Steady-state Stern-Volmer plot of the integrate fluorescence intensity ratio (F_0/F) as a function of quencher concentration. **d** Steady-state modified Stern-Volmer plot of the integrated fluorescence intensity ratio ($F_0/(F_0-F)$) and as a function of $1/[Q]$

dsDNA complex through fluorescence quenching studies, as is demonstrated below in the "Fluorescence quenching of the SYBR Green I-DNA complex by the MILs" and "Fluorescence quenching of the SYBR Green I-DNA complex by the metal salts" sections.

Fluorescence quenching of the SYBR Green I-DNA complex by the MILs

In order to ensure that all of the SYBR Green I dye was bound to dsDNA and that the two populations of fluorophores observed were not from quencher molecules interacting with excess of SYBR Green I, the fluorescence intensity of 1.96 μM SYBR Green I with 1 nM, 3.5 nM and 10 nM of dsDNA (in absence of any quencher) was recorded (Fig. S5 of the ESM). A Student's t-test concluded that the integrated fluorescence intensities of the corrected spectra for 1.96 μM SYBR Green I with 1-nM dsDNA compared to the 3.5 nM and 10 nM dsDNA were not statistically different (see Table S1 of the ESM). This result indicates that all of the SYBR Green I dye in solution is bound to the dsDNA, and that the two populations of fluorophores observed in the quenching experiments were from two different populations of the SYBR Green I-dsDNA complex accessible to the quencher molecules. Thus, 1 nM dsDNA was used for all quenching experiments.

As previously mentioned, Figs. 2, 3, and 4 show the steady-state Stern-Volmer plots and modified Stern-Volmer plots for the fluorescence quenching of the SYBR Green I-dsDNA complex by the $[Ni(BIm)_4^{2+}]2[Cl^-]$, $[Ni(BnIm)_4^{2+}]2[Cl^-]$ and $[Co(BIm)_4^{2+}]2[Cl^-]$ MILs. The modified Stern-Volmer plots were fit to Eq. (3) and the quenching parameters are presented in Table 2. From the intercept, values of 0.73 ± 0.02 and 0.69 ± 0.02 were obtained for f_a for the $[Ni(BIm)_4^{2+}]2[Cl^-]$ and $[Ni(BnIm)_4^{2+}]2[Cl^-]$ MILs, respectively. This result indicates that approximately 69–73% of the SYBR Green I-dsDNA complex was accessible for quenching by the Ni(II)-based MILs and the other 27–31% was not affected by the MILs added at increasing concentrations (Figs. 2 and 3). On the other hand, the intercept of the modified Stern-Volmer plot for the $[Co(BIm)_4^{2+}]2[Cl^-]$ MIL yielded a f_a value of 0.97 ± 0.01, indicating that the majority of the SYBR Green I-dsDNA complex was available to the $[Co(BIm)_4^{2+}]2[Cl^-]$ MIL quencher over the concentration

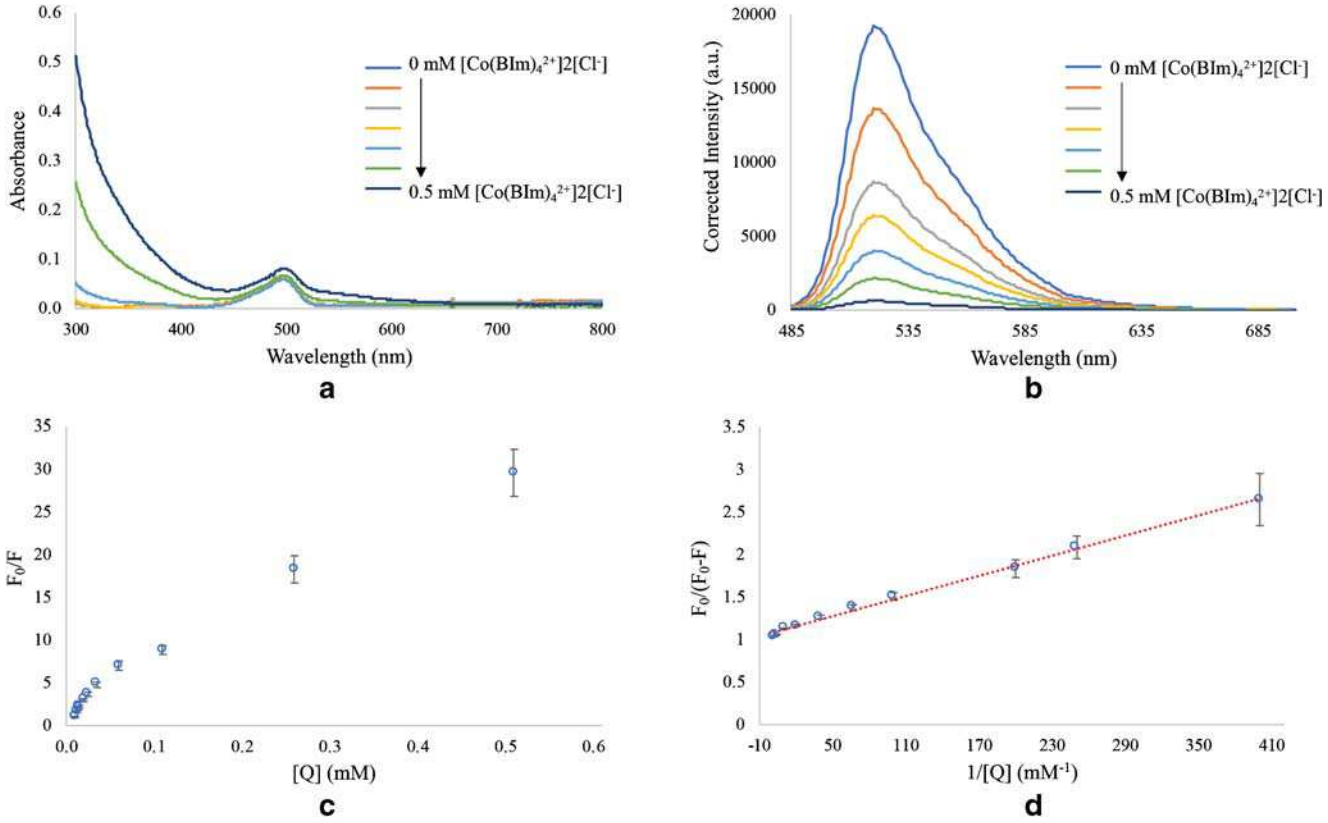

Fig. 4 Fluorescence quenching of the SYBR Green I-dsDNA complex as a function of $[Co(BIm)_4^{2+}]2[Cl^-]$ concentration. **a** Absorption spectra. **b** Fluorescence emission spectra, $\lambda_{ex} = 475$ nm. Intensities were corrected for the absorption at the wavelength of excitation. **c** Steady-state Stern-Volmer plot of the integrate fluorescence intensity ratio (F_0/F) as a function of quencher concentration. **d** Steady-state modified Stern-Volmer plot of the integrated fluorescence intensity ratio ($F_0/(F_0\text{-}F)$) and as a function of $1/[Q]$

range of 0 to 0.5 mM. As described in the "Quantifying fluorescence quenching of the SYBR Green I-DNA complex" section, the quenching constants of the accessible fraction, K_a, were 100 ± 20, 120 ± 20, and 200 ± 20 mM^{-1} for the $[Ni(BIm)_4^{2+}]2[Cl^-]$, $[Ni(BnIm)_4^{2+}]2[Cl^-]$, and $[Co(BIm)_4^{2+}]2[Cl^-]$ MILs, respectively (see Table 2).

With regard to the two studied Ni(II)-based MILs ($[Ni(BIm)_4^{2+}]2[Cl^-]$ and $[Ni(BnIm)_4^{2+}]2[Cl^-]$), the f_a and K_a values can be considered equal within experimental error (see Table 2). However, a change in the absorption spectrum of the SYBR Green I-dsDNA complex at higher concentrations of the $[Ni(BnIm)_4^{2+}]2[Cl^-]$ MIL was observed, as shown in Fig. 3. This possibly indicates static quenching owing to complex formation between the SYBR Green I-dsDNA and the $[Ni(BnIm)_4^{2+}]2[Cl^-]$ MIL. The BnIm ligand of the MIL can interact with dsDNA through π-π stacking interactions, forming a non-fluorescent ground-state complex, conducive to static quenching [28, 40].

Table 1 Förster critical distances (R_0) of the metal salts and MILs obtained using Eq. (5)

Quencher	R_0 (Å)
$NiCl_2$	9.00
$CoCl_2$	14.1
$[Ni(BIm)_4^{2+}]2[Cl^-]$	11.9
$[Ni(BnIm)_4^{2+}]2[Cl^-]$	13.9
$[Co(BIm)_4^{2+}]2[Cl^-]$	18.8

Fluorescence quenching of the SYBR Green I-DNA complex by the metal salts

In an attempt to understand how the MILs quench the fluorescence of SYBR Green I-dsDNA complex, their Stern-Volmer plots were compared with those using the "bare" ions obtained from the salts, $NiCl_2$ and $CoCl_2$ (ESM Figs.

Table 2 The fraction of fluorescence accessible to the quencher (f_a) and the Stern-Volmer quenching constant of the accessible fraction (K_a) for the metal salts and MILs obtained using Eq. (3)

Quencher	f_a	K_a (mM^{-1})
$NiCl_2$	0.61 ± 0.01	160 ± 10
$CoCl_2$	0.93 ± 0.01	180 ± 10
$[Ni(BIm)_4^{2+}]2[Cl^-]$	0.73 ± 0.02	100 ± 20
$[Ni(BnIm)_4^{2+}]2[Cl^-]$	0.69 ± 0.02	120 ± 20
$[Co(BIm)_4^{2+}]2[Cl^-]$	0.97 ± 0.01	200 ± 20

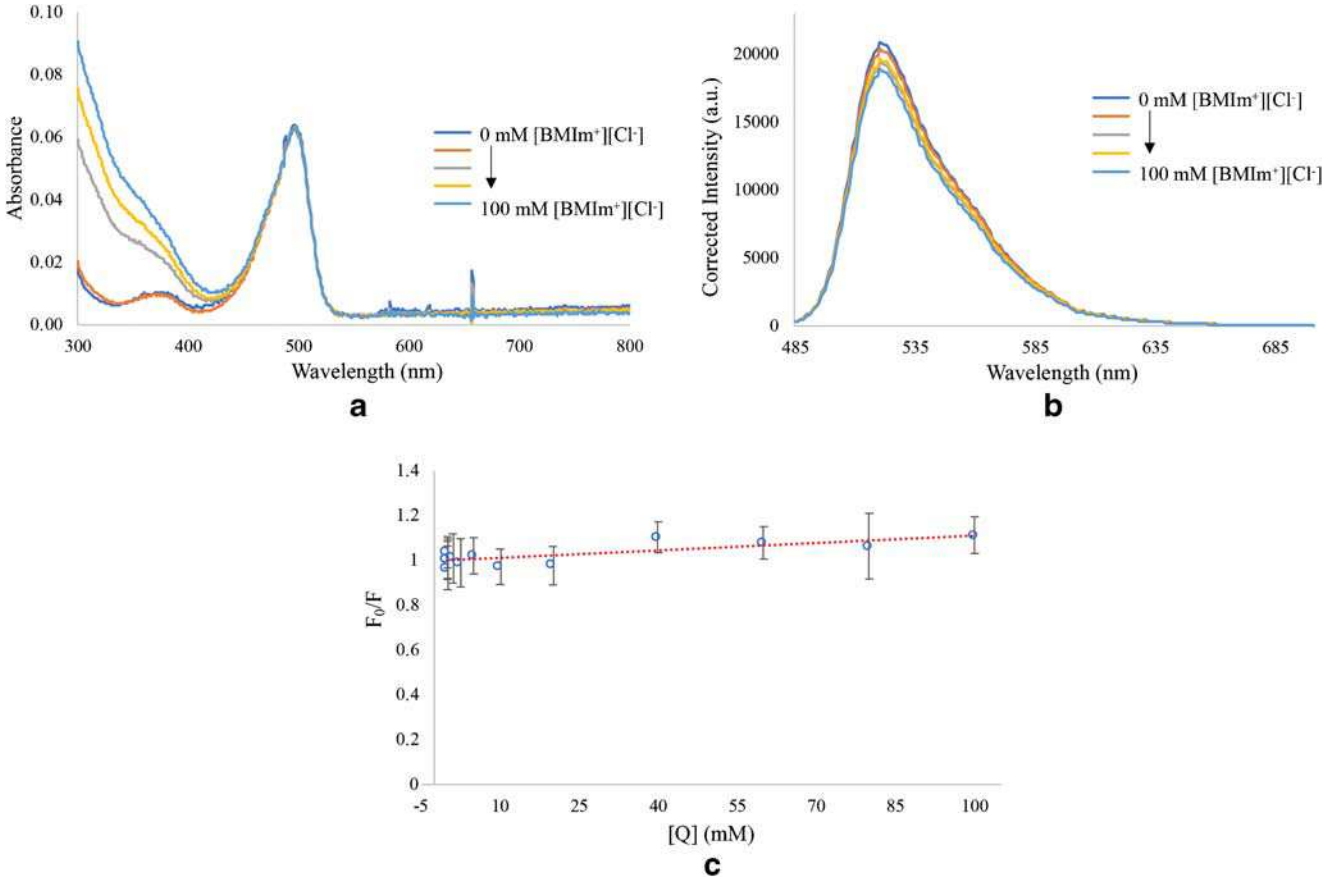

Fig. 5 Fluorescence quenching of the SYBR Green I-dsDNA complex as a function of $[BMIm^+][Cl^-]$ concentration. **a** Absorption spectra. **b** Fluorescence emission spectra, $\lambda_{ex} = 475$ nm. Intensities were corrected for the absorption at the wavelength of excitation. **c** Steady-state Stern-Volmer plot of the integrate fluorescence intensity ratio (F_0/F) as a function of quencher concentration

S2 and S3). These plots exhibited the same deviation from linearity towards the "x-axis" as those of the MILs, and, therefore, they were also fit using Eq. (3). Results are summarized in Table 2. Within experimental error, Co^{2+} is a more efficient quencher than Ni^{2+}: $K_a = 180 \pm 10$ mM^{-1} as opposed to 160 ± 10 mM^{-1}. This difference may be attributed to the greater accessibility of Co^{2+} with respect to that of Ni^{2+}: 0.93 as opposed to 0.61.

$NiCl_2$ has an accessibility similar to those of the $[Ni(BIm)_4^{2+}]2[Cl^-]$ and $[Ni(BnIm)_4^{2+}]2[Cl^-]$ MILs, within experimental error: 061 ± 0.01 as opposed to 0.73 ± 0.02 and 0.69 ± 0.69. On the other hand, its K_a is larger: 160 ± 10 mM^{-1} for $NiCl_2$; but 100 ± 20 mM^{-1} and 120 ± 20 mM^{-1} for the two MILs, respectively. In contrast, $CoCl_2$ and $[Co(BIm)_4^{2+}]2[Cl^-]$ have similar f_a and K_a values within experimental error. It should be noted that the presence of the ligands do not affect the f_a and K_a of Co^{2+}, whereas they have a significant on Ni^{2+}. This suggests that the coordination of the ligands in the Co^{2+} and Ni^{2+} MILs is different.

As noted in the "Evaluation of the contribution of Förster resonance energy transfer (FRET) to fluorescence quenching" section, the R_0 values of the metal salts and MILs were all below 20 Å. Therefore, FRET is likely not a main contributor to the quenching effect and the mechanism of quenching must either be through spin-orbit coupling or excited-state electron transfer. There could be a difference in quenching depending on the geometry of the MIL in solution although this also lies beyond the scope of the current study and was not investigated in further detail.

Effect of the IL (no metal) control on the fluorescence of the SYBR Green I-DNA complex

To study the effect of a non-magnetic IL on the fluorescence of the SYBR Green I-dsDNA complex, Stern-Volmer plots were obtained by adding 0 to 100 mM of the $[BMIm^+][Cl^-]$ IL to the SYBR Green I-dsDNA complex. As shown in Fig. 5, the Stern-Volmer plot was linear and fit to Eq. (3), yielding a K_{SV} of 1.2 ± 0.2 M^{-1}. This indicates that the $[BMIm^+][Cl^-]$ IL has a negligible effect on the fluorescence of the SYBR Green I-dsDNA complex, and that the metal ions in the cation of the MIL structure are mainly responsible for the fluorescence quenching of the complex.

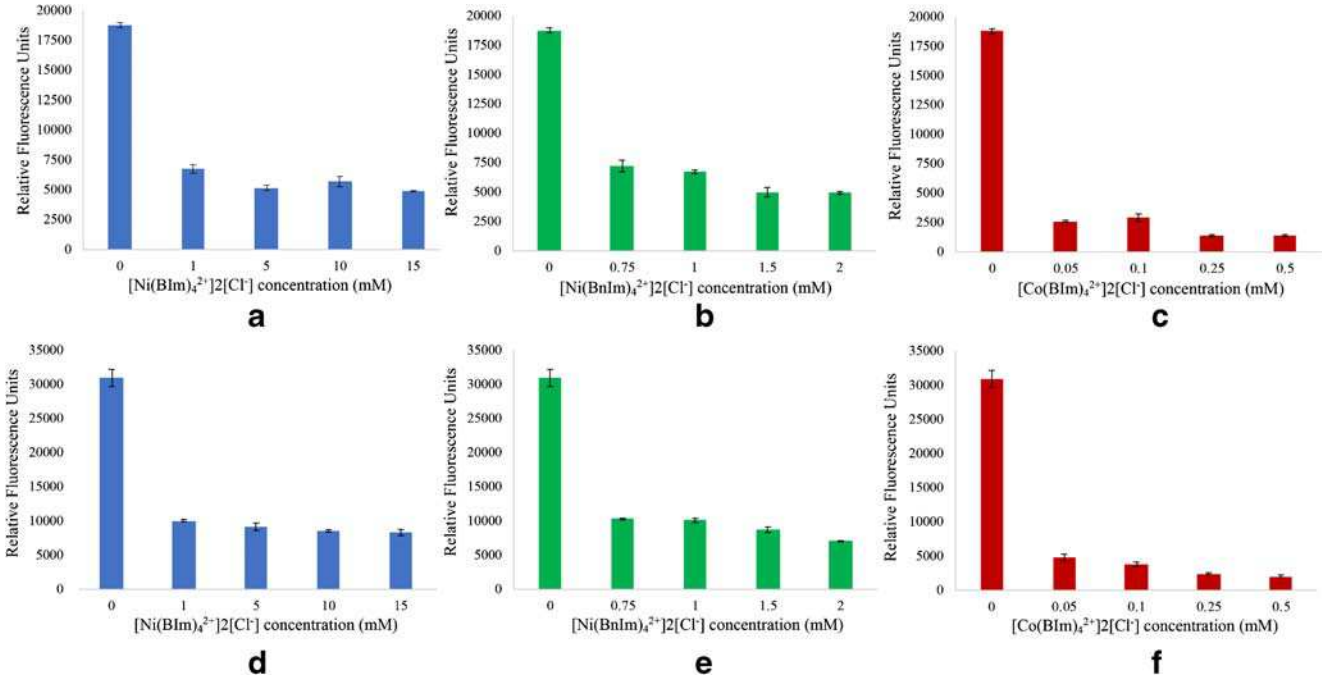

Fig. 6 qPCR and fluorescence emission measurements of mixtures of MIL and the SYBR Green I-dsDNA complex. The measurements were recorded using the four highest MIL concentrations employed in constructing the Stern-Volmer plots. **a** 0, 1, 5, 10, and 15 mM $[Ni(BIm)_4^{2+}]2[Cl^-]$ MIL using qPCR detection, **b** 0, 0.75, 1, 1.5, and 2 mM $[Ni(BnIm)_4^{2+}]2[Cl^-]$ MIL using qPCR detection, **c** 0, 0.05, 0.1, 0.25, and 0.5 mM $[Co(BIm)_4^{2+}]2[Cl^-]$ MIL using qPCR detection, **d** 0, 1, 5, 10, and 15 mM $[Ni(BIm)_4^{2+}]2[Cl^-]$ MIL using fluorescence emission detection, **e** 0, 0.75, 1, 1.5, and 2 mM $[Ni(BnIm)_4^{2+}]2[Cl^-]$ MIL using fluorescence emission detection, **f** 0, 0.05, 0.1, 0.25, and 0.5 mM $[Co(BIm)_4^{2+}]2[Cl^-]$ MIL using fluorescence emission

Applicability of MILs for direct use in fluorescence-based assays

The final objective of this study is to determine if the MILs can be directly applied to fluorescence-based bioanalytical techniques such as qPCR and fluorescence emission measurements recorded with a microplate reader. The four highest concentrations of each MIL employed in the Stern-Volmer plots (1 to 15 mM for the $[Ni(BIm)_4^{2+}]2[Cl^-]$ MIL, 0.75 to 2 mM for the $[Ni(BnIm)_4^{2+}]2[Cl^-]$ MIL and 0.05 to 0.5 mM for the $[Co(BIm)_4^{2+}]2[Cl^-]$ MIL) were added to the SYBR Green I-dsDNA complex. A fluorescence signal was able to be detected in both qPCR and fluorescence emission measurements with a microplate reader at the highest concentrations of each MIL, as shown in Fig. 6. These results indicate that the MILs can be directly used at these or lower concentrations in qPCR and fluorescence emission measurements with microplate readers with SYBR Green I-dsDNA as the fluorophore complex.

Conclusions

In this study, MILs containing the paramagnetic component in the cation and chloride anions were used in absorption and fluorescence emission spectroscopy to evaluate their suitability for use in fluorescence-based DNA applications. The SYBR Green I-dsDNA complex was used as the fluorophore in the assessment of the fluorescence quenching effects of the MILs themselves, as well as metal chloride salts and a non-magnetic IL for comparison.

As predicted and confirmed through fluorescence quenching experiments, the metal (Co^{2+} or Ni^{2+}) of the MIL was the main component in the structure responsible for quenching of the fluorescence signal. As increasing concentration of quencher was added, it was found that the SYBR Green I-dsDNA complex provided an environment where two populations of fluorophores were present, both with different accessibilities to the quencher. This behavior was observed for all of the MILs and the metal chloride salts. This new generation of MILs exhibited large quenching constants, as observed by a significant reduction in the fluorescent signal when increasing amounts were added to the SYBR Green I-dsDNA complex. The results from this study cannot distinguish between the two quenching mechanisms of these MILs as being spin-orbit coupling or excited-state electron transfer. Owing to the small overlap integral between the absorption spectrum of each MIL and the emission spectrum of the SYBR Green I-dsDNA complex, it can be concluded that non-radiative Förster resonance energy transfer is not significant. Although large quenching constants were observed for the MILs with SYBR Green I-dsDNA as the fluorescent probe, they were still able to be used directly in qPCR and fluorescence emission measurements using a microplate reader at the four

highest concentrations found in each Stern-Volmer plot, indicating that these MILs can be used in fluorescence-based assays.

The $[Ni(BIm)_4^{2+}]2[Cl^-]$ and $[Ni(BnIm)_4^{2+}]2[Cl^-]$ MILs quenched fluorescence identically within experimental error. Careful observation, however, of the absorption spectra of the SYBR Green I-dsDNA complex with the $[Ni(BnIm)_4^{2+}]2[Cl^-]$ MIL revealed a possible static quenching component, thereby rendering the use of the $[Ni(BIm)_4^{2+}]2[Cl^-]$ MIL in fluorescence-based assays as possibly more advantageous. In PCR experiments, customized PCR buffers can be designed to alleviate inhibition caused by the MILs if they are used in DNA extractions and directly added to the PCR buffer. This is similar to what was performed with previous generations of MILs which contained the metal in the anion [15, 25].

Acknowledgments J. L. A. acknowledges funding from the Chemical Measurement and Imaging Program at the National Science Foundation (CHE-1709372).

Compliance with ethical standards

Conflict of interest The authors declare that they have no conflict of interest.

Research involving human participants and/or animals informed consent This article does not contain any studies with human participants or animals performed by any of the authors.

References

1. Yershov G, Barsky V, Belgovskiy A, Kirillov E, Kreindlin E, Ivanov I, et al. DNA analysis and diagnostics on oligonucleotide microchips. Proc Natl Acad Sci U S A. 1996;93(10):4913–8. https://doi.org/10.1073/pnas.93.10.4913.
2. Evans WE, Relling MV. Moving towards individualized medicine with pharmacogenomics. Nature. 2004;429(6990):464–8. https://doi.org/10.1038/nature02626.
3. Butler JM. The future of forensic DNA analysis. Philos Trans R Soc B Biol Sci. 1674;2015(370). https://doi.org/10.1098/rstb.2014.0252.
4. Newman ME, Parboosingh JS, Bridge PJ, Ceri H. Identification of archaeological animal bone by PCR/DNA analysis. J Archaeol Sci. 2002;29(1):77–84. https://doi.org/10.1006/jasc.2001.0688.
5. Auricchio B, Anniballi F, Fiore A, Skiby JE, De Medici D. Evaluation of DNA extraction methods suitable for PCR-based detection and genotyping of Clostridium botulinum. Biosecur Bioterror. 2013;11(1):200–6. https://doi.org/10.1089/bsp.2012.0082.
6. Nishi K, Isobe SI, Zhu Y, Kiyama R. Fluorescence-based bioassays for the detection and evaluation of food materials. Sensors. 2015;15(10):25831–67. https://doi.org/10.3390/s151025831.
7. Green MR, Sambrook J. Molecular cloning: a laboratroy manual. 4th ed. Cold Springs Harbor: Cold Springs Harbor Laboratory Press; 2012.
8. Tan SC, Yiap BC. DNA, RNA, and protein extraction: the past and the present. J Biomed Biotechnol. 2009;2009:1–10. https://doi.org/10.1155/2009/574398.
9. Lienhard A, Schäffer S. Extracting the invisible: obtaining high quality DNA is a challenging task in small arthropods. PeerJ. 2019;7:1–17. https://doi.org/10.7717/peerj.6753.
10. Gumińska N, Płecha M, Walkiewicz H, Hałakuc P, Zakryś B, Milanowski R. Culture purification and DNA extraction procedures suitable for next-generation sequencing of Euglenids. J Appl Phycol. 2018;30(6):3541–9. https://doi.org/10.1007/s10811-018-1496-0.
11. Wang JH, Cheng DH, Chen XW, Du Z, Fang ZL. Direct extraction of double-stranded DNA into ionic liquid 1-butyl-3-methylimidazolium hexafluorophosphate and its quantification. Anal Chem. 2007;79(2):620–5. https://doi.org/10.1021/ac061145c.
12. Li T, Joshi MD, Ronning DR, Anderson JL. Ionic liquids as solvents for in situ dispersive liquid-liquid microextraction of DNA. J Chromatogr A. 2013;1272:8–14. https://doi.org/10.1016/j.chroma.2012.11.055.
13. Clark KD, Nacham O, Yu H, Li T, Yamsek MM, Ronning DR, et al. Extraction of DNA by magnetic ionic liquids: tunable solvents for rapid and selective DNA analysis. Anal Chem. 2015;87(3):1552–9. https://doi.org/10.1021/ac504260t.
14. Clark KD, Sorensen M, Nacham O, Anderson JL. Preservation of DNA in nuclease-rich samples using magnetic ionic liquids. RSC Adv. 2016;6(46):39846–51. https://doi.org/10.1039/c6ra05932e.
15. Emaus MN, Clark KD, Hinners P, Anderson JL. Preconcentration of DNA using magnetic ionic liquids that are compatible with real-time PCR for rapid nucleic acid quantification. Anal Bioanal Chem. 2018:4135–44. https://doi.org/10.1007/s00216-018-1092-9.
16. Clark KD, Varona M, Anderson JL. Ion-tagged oligonucleotides coupled with a magnetic liquid support for the sequence-specific capture of DNA. *Angew Chem Int Ed Eng*. 2017;56(26):7630–3. https://doi.org/10.1002/anie.201703299.
17. Marengo A, Cagliero C, Sgorbini B, Anderson JL, Emaus MN, Bicchi C, et al. Development of an innovative and sustainable one-step method for rapid plant DNA isolation for targeted PCR using magnetic ionic liquids. Plant Methods. 2019;15(1):1–11. https://doi.org/10.1186/s13007-019-0408-x.
18. Clark KD, Emaus MN, Varona M, Bowers AN, Anderson JL. Ionic liquids: solvents and sorbents in sample preparation. *J Sep Sci*. **2018**;*41*(1). https://doi.org/10.1002/jssc.201700864.
19. Santos E, Albo J, Irabien A. Magnetic ionic liquids: synthesis, Properties and Applications. *RSC Adv*. 2014;4(75):40008–18. https://doi.org/10.1039/c4ra05156d.
20. Clark KD, Nacham O, Purslow JA, Pierson SA, Anderson JL. Magnetic ionic liquids in analytical chemistry: a review. Anal Chim Acta. 2016;934:9–21. https://doi.org/10.1016/j.aca.2016.06.011.
21. Trujillo-Rodríguez MJ, Nan H, Varona M, Emaus MN, Souza ID, Anderson JL. Advances of ionic liquids in analytical chemistry. Anal Chem. 2019;91(1):505–31. https://doi.org/10.1021/acs.analchem.8b04710.
22. Sajid M. Magnetic ionic liquids in analytical sample preparation: a literature review. *TrAC Trends Anal Chem*. 2019;113:210–23. https://doi.org/10.1016/j.trac.2019.02.007.
23. Hallett JP, Welton T. Room-temperature ionic liquids: solvents for synthesis and catalysis. 2. Chem Rev. 2011;111(5):3508–76. https://doi.org/10.1021/cr1003248.
24. Bowers AN, Trujillo-Rodríguez MJ, Farooq MQ, Anderson JL. Extraction of DNA with magnetic ionic liquids using in situ dispersive liquid – liquid microextraction. Anal Bioanal Chem. 2019;411:7375–85. https://doi.org/10.1007/s00216-019-02163-9.
25. Clark KD, Yamsek MM, Nacham O, Anderson JL. Magnetic ionic liquids as PCR-compatible solvents for DNA extraction from biological samples. Chem Commun. 2015;51(94):16771–3. https://doi.org/10.1039/c5cc07253k.
26. Santra K, Clark KD, Maity N, Petrich JW, Anderson JL. Exploiting fluorescence spectroscopy to identify magnetic ionic liquids

suitable for the isolation of oligonucleotides. J Phys Chem B. 2018;122:7747–56. https://doi.org/10.1021/acs.jpcb.8b05580.
27. Fleming GR. Chemical applications of ultrafast spectroscopy. New York: Oxford University Press; 1986.
28. Lakowicz JR. Principles of fluorescence spectroscopy. 3rd ed. New York: Springer; 2006.
29. Stern O, Volmer M. Über die Abklingzeit der Fluoreszenz. *Phys Z.* **1919**;*20*(183).
30. Varnes AW, Dodson RB, Wehry EL. Interactions of transition-metal ions with photoexcited states of Flavins. Fluorescence quenching studies. *J Am Chem Soc*. 1972;94(3):946–50. https://doi.org/10.1021/ja00758a037.
31. Yue Q, Hou Y, Yue S, Du K, Shen T, Wang L, et al. Construction of an off-on fluorescence system based on carbon dots for trace pyrophosphate sensing. J Fluoresc. 2015;25(3):585–94. https://doi.org/10.1007/s10895-015-1538-9.
32. Yao C, Anderson JL. Dispersive liquid-liquid microextraction using an in situ metathesis reaction to form an ionic liquid extraction phase for the preconcentration of aromatic compounds from water. Anal Bioanal Chem. 2009;395(5):1491–502. https://doi.org/10.1007/s00216-009-3078-0.
33. Chand D, Farooq MQ, Pathak AK, Li J, Smith EA, Anderson JL. Magnetic ionic liquids based on transition-metal complexes with N-alkylimidazole ligands. New J Chem. 2019;43:20–3. https://doi.org/10.1039/C8NJ05176C.
34. Fraiji LK, Hayes DM, Werner TC. Static and dynamic fluorescence quenching experiments for the physical chemistry laboratory. J Chem Educ. 1992;69(5):424. https://doi.org/10.1021/ed069p424.
35. Lehrer SS. Solute Perturbation of protein fluorescence. The quenching of the tryptophyl fluorescence of model compounds and of lysozyme by iodide ion. Biochemistry. 1971;10(17):3254–63. https://doi.org/10.1021/bi00793a015.
36. Keizer J. Nonlinear fluorescence quenching and the origin of positive curvature in Stern-Volmer plots. J Am Chem Soc. 1983;105(6):1494–8. https://doi.org/10.1021/ja00344a013.
37. Wang YQ, Zhang HM, Zhang GC, Tao WH, Tang SH. Interaction of the flavonoid hesperidin with bovine serum albumin: a fluorescence quenching study. J Lumin. 2007;126(1):211–8. https://doi.org/10.1016/j.jlumin.2006.06.013.
38. Xing D, Dorr R, Cunningham RP, Scholes CP. Endonuclease III interactions with DNA substrates. 2. The DNA repair enzyme endonuclease III binds differently to intact DNA and to apyrimidinic/apurinic DNA substrates as shown by tryptophan fluorescence quenching. Biochemistry. 1995;34(8):2537–44. https://doi.org/10.1021/bi00008a018.
39. Förster T. Transfer mechanisms of electronic excitation energy. Radiat Res Suppl. 1960;2:326–39.
40. Hunter CA, Sanders JKM. The nature of π-π interactions. J Am Chem Soc. 1990;112(14):5525–34. https://doi.org/10.1021/ja00170a016.

Ashley N. Bowers completed her M.S. in analytical chemistry from Iowa State University in December 2019. Her research involved studying magnetic ionic liquids and nucleic acid interactions in Professor Anderson's research group. She is currently working in industry.

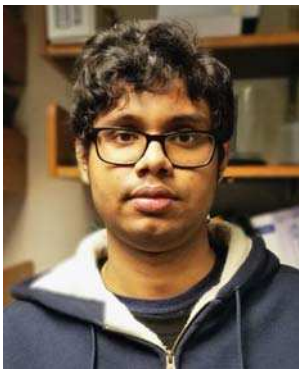

Kalyan Santra received his Ph.D. in Physical Chemistry in 2018 from Iowa State University. He is currently working as Postdoctoral Research Associate in the Division of Chemical and Biological Sciences at Ames Laboratory, in Professor Jacob W. Petrich's and Professor Xueyu Song's groups. He has been working on the development and applications of spectroscopy and microscopy techniques.

María J. Trujillo-Rodríguez obtained her Ph.D. in Chemistry in 2017 in Universidad de La Laguna, Spain. She worked as Postdoctoral Research Associate in Professor Anderson's research group in Iowa State University from 2017 to 2019, and she is currently working at Universitat de les Illes Balears, Spain. Her research interests include the development of new microextraction procedures using ionic liquids and derivatives for environmental and food analysis.

Anthony Song is completing a B.S. in Chemistry and Data Science at Iowa State University. His research interests involve the development of new spectroscopic techniques for environmental and physiological analysis.

Jacob W. Petrich has been on the faculty of the Department of Chemistry at Iowa State University since 1989, where he is currently a Professor and a Faculty Scientist with the Ames Laboratory, U.S. Department of Energy. His interests lie in time-resolved spectroscopy and super-resolution imaging.

Miranda N. Emaus received her B.S. in chemistry and forensic chemistry from Lake Superior State University, Sault Ste. Marie, Michigan. She is currently a graduate student studying analytical chemistry under the supervision of Dr. Jared L. Anderson at Iowa State University. Her research involves the application of magnetic ionic liquids towards nucleic acid analysis.

Jared L. Anderson is the Alice Hudson Professor of Chemistry at Iowa State University and also Faculty Scientist with the Ames Laboratory, U.S. Department of Energy. His research focuses on the development of stationary phases for multidimensional chromatography, alternative approaches for sample preparation, particularly in nucleic acid isolation and purification, and developing analytical tools for trace-level analysis within active pharmaceutical ingredients.